J. Fluid Mech. (2010), *vol.* 656, *pp.* 189–204.
doi:10.1017/S0022112010001126

Fast forced liquid film spreading on a substrate: flow, heat transfer and phase transition

ILIA V. ROISMAN†

Technische Universität Darmstadt, Chair of Fluid Mechanics and Aerodynamics, Center of Smart Interfaces, Petersenstrasse 30, 64287 Darmstadt, Germany

(Received 13 April 2009; revised 28 February 2010; accepted 28 February 2010; first published online 21 May 2010)

This theoretical study is devoted to description of fluid flow and heat transfer in a spreading viscous drop with phase transition. A similarity solution for the combined full Navier–Stokes equations and energy equation for the expanding lamella generated by drop impact is obtained for a general case of oblique drop impact with high Weber and Reynolds numbers. The theory is applicable to the analysis of the phenomena of drop solidification, target melting and film boiling. The theoretical predictions for the contact temperature at the substrate surface agree well with the existing experimental data.

1. Introduction

The flow produced by isothermal drop impact onto a dry substrate is governed by inertial, viscous and capillary effects. The main dimensionless parameters determining the outcome of drop impact are therefore the Reynolds number, $Re = D_0 W_0/\nu$, and the Weber number, $We = \rho D_0 W_0^2/\sigma$, where D_0 and W_0 are the initial drop diameter and impact velocity, ν, ρ and σ are the kinematic viscosity, density and surface tension, respectively. If the Weber number is small, the wettability of the surface also affects the drop spreading (Bico, Marzolin & Quéré 1999; Mock *et al.* 2005). The target properties, for example, its shape (Bakshi, Roisman & Tropea 2007), roughness (Range & Feuillebois 1998), elasticity (Pepper, Courbin & Stone 2008) or porosity (Kellay 2005), can influence the liquid flow and even enhance or reduce splashing.

Comprehensive reviews of studies in the field of drop impact can be found in Rein (2000), Tropea & Roisman (2005), Ukiwe & Kwok (2005), Yarin (2006) and elsewhere. Yarin & Weiss (1995) investigated experimentally and modelled periodic impact and splash produced by a train of drops. Their important theoretical results are also highly relevant to the description of a single drop impact onto a dry substrate with high Reynolds and high Weber numbers. In particular, recent experiments (Bakshi *et al.* 2007) show that the remote asymptotic solution developed by Yarin & Weiss (1995) predicts well the flow distribution in the expanding lamella and the evolution of its thickness. Roisman, Berberović & Tropea (2009) show that at high Weber and Reynolds numbers the thickness evolution of the expanding lamella is almost not influenced by the liquid viscosity or surface tension. In Roisman (2009) a self-similar solution of the full Navier–Stokes equations for isothermally spreading viscous lamella has been obtained. This solution allows us to predict the residual film thickness formed by drop impact and maximum spreading diameter.

† Email address for correspondence: roisman@sla.tu-darmstadt.de

Flow in a spreading drop determines not only the outcome of drop impact and the residual film thickness. In some applications, for example in the case of inkjet printing of microarrays of bio-molecules (Dijksman & Pierik 2008), the flow in a spreading drop transports the capture probes on the surface of a solid support and determines the quality of the array.

The phenomena of non-isothermal drop impact is much more complicated, since additional influencing parameters related to heat transfer and to the temperature dependence of the material properties have to be accounted for. In many cases drop spreading is followed by various phase change processes in the near-wall region, including drop solidification, vaporization and substrate melting.

Solidification of a spreading drop and remelting of target are the phenomena relevant to the technology of spray forming (Orme 1993), plasma spray coating (Fauchais *et al.* 2004), surface mount technologies (Attinger, Zhao & Poulikakos 2000), microfabrication (Steirer *et al.* 2009) and inkjet printing. The mechanism of spreading and solidification of supercooled drops on an aircraft wing determines the process of ice accretion (Miller, Lynch & Tate 2002), which can influence the aerodynamics of the aircraft.

The hydrodynamics and heat transfer of a spreading drop determine the geometry of splat, its thickness and diameter. Drop solidification in some cases (if the Weber and Reynolds numbers are high enough) can enhance the flow instability and lead to splash (Dhiman & Chandra 2005). When the initial drop temperature is high enough, drop impact can lead to the substrate remelting (Amon *et al.* 1996).

The study of drop impact and its vaporization on a very hot surface is relevant to spray cooling, to interaction of spray with walls of internal combustion engines and to spray/wall interactions during atomization in air-blast atomizers in gas turbines. If the substrate temperature is above the Leidenfrost point, a thin vapour layer is created, preventing a direct contact between the liquid and the solid substrate. This phenomenon, called film boiling, influences significantly the outcome of the drop impact.

The outcome of drop impact is only very slightly influenced by the wall temperature if it is below the Leidenfrost temperature. At the Leidenfrost temperature the flow changes significantly. Various breakup modes observed in experiments of Senda *et al.* (1988) at various surface temperatures and impact parameters can be subdivided onto (i) rebound, (ii) breakup and rebound, (iii) breakup due to the vapour blowing through the liquid lamella, (iv) droplet ejection from the upper surface of the lamella, (v) complete lamella disintegration, (vi) complete lamella disintegration followed by the very fast radial motion of the fragments. Generally, when the initial wall temperature increases, the breakup of the impacting drop onto a myriad of very small secondary droplets happens earlier (Manzello & Yang 2002).

The fundamentals of the near-wall liquid vaporization (Carey 2007) and solidification (Worster 2000) are well known. However, the problem which considers instationary, non-axisymmetric flow in a fast spreading drop, instationary temperature field in the liquid and solid regions and phase transition in the near-wall region has not been yet solved analytically. If a drop impacts onto a solid surface it generates a radially expanding flow in a lamella bounded by a rim. The dynamics of the rim is determined by surface tension, inertia of the liquid entering the rim from the lamella and forces associated with wettability. If the impact velocity is high enough, i.e. the Reynolds and Weber numbers are much higher than unity, the rim motion does not influence the flow in the lamella (Roisman *et al.* 2009). The present study is focused on the theoretical description of the hydrodynamics, heat transfer and phase change

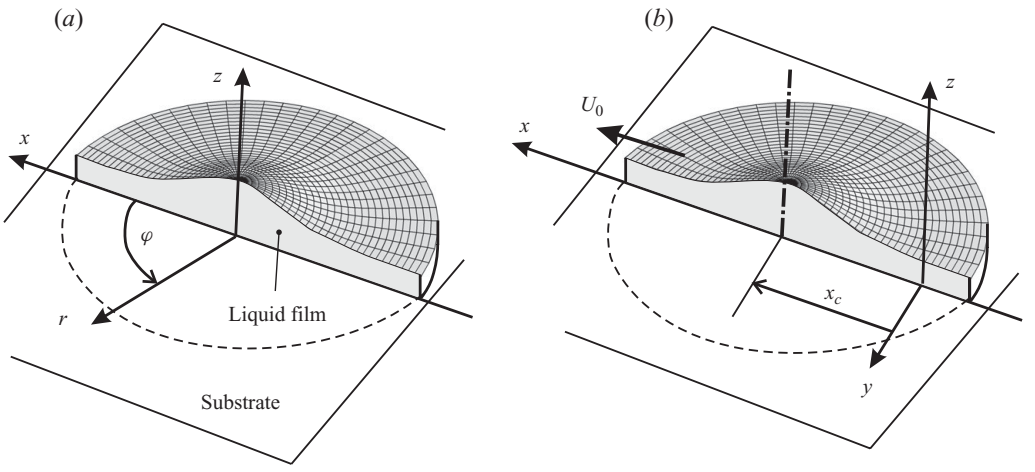

FIGURE 1. Sketches of an axisymmetric spreading film (*a*) and of non-axisymmetric spreading film (*b*) generated by drop impact.

in a spreading liquid film applicable to the flow in the lamella generated by normal or inclined drop impact. We obtain a similarity solution for the combined continuity, full Navier–Stokes and energy equations in the case when the thermodynamic parameters of the materials depend on the local temperature, phase state and material. The theory is able to predict the rate of propagation of the phase transition front, heat fluxes at the interfaces and contact temperatures. The theoretical predictions for the contact temperature at the surface of the solid substrate agrees well with the experimental data. The analysis explains the heat transfer enhancement associated with the film spreading.

2. Remote asymptotic solution for the flow in a spreading lamella

Consider a normal drop impact onto a planar rigid wall (see figure 1*a*). If the Reynolds and Weber numbers are high, the radially expanding flow in the lamella can be described well in the cylindrical coordinate system $\{r, \varphi, z\}$ with the unit base vectors $\{\boldsymbol{e}_r, \boldsymbol{e}_\varphi, \boldsymbol{e}_z\}$ by the remote asymptotic solution (Yarin & Weiss 1995)

$$\boldsymbol{v}_0 = \frac{r\boldsymbol{e}_r - 2z\boldsymbol{e}_z}{t+\tau}. \tag{2.1}$$

In the case of oblique drop impact the flow is no longer axisymmetric, since the initial transverse component of the impact velocity initiates a translational motion in the x direction. Consider now a Cartesian coordinate system $\{x, y, z\}$ with the unit base vectors $\{\boldsymbol{e}_x, \boldsymbol{e}_y, \boldsymbol{e}_z\}$, shown in figure 1(*b*). In this coordinate system the drop impact velocity is represented as $\boldsymbol{V} = -W_0\boldsymbol{e}_z + U_0\boldsymbol{e}_x$, where W_0 and U_0 are the normal and tangential components of the impact velocity. The inviscid flow in the lamella generated by inclined drop impact can be obtained as a translation of the axisymmetric flow (2.1) with the velocity $U_0\boldsymbol{e}_x$ (Roisman & Tropea 2002). The resulting flow can be written in the Cartesian coordinate system as

$$\boldsymbol{v}_0 = \frac{(x-x_c)\boldsymbol{e}_x + y\boldsymbol{e}_y - 2z\boldsymbol{e}_z}{t+\tau} + U_0\boldsymbol{e}_x, \quad x_c = U_0 t. \tag{2.2}$$

In the numerical simulations of normal drop impact (Roisman *et al.* 2009), it was shown that the value of the constant τ does not depend on the impact parameters and is of order $\tau \approx 0.25 D_0/W_0$. It is therefore much smaller than the characteristic time of drop impact D_0/W_0 and can be neglected at long times after impact. The remote asymptotic solution for the flow in the lamella is therefore

$$\boldsymbol{v}_0 = \frac{(x + U_0\tau)\boldsymbol{e}_x + y\boldsymbol{e}_y - 2z\boldsymbol{e}_z}{t}. \tag{2.3}$$

It can be shown that this flow satisfies exactly the continuity and momentum balance equations even if the liquid viscosity is significant. However, this velocity field does not satisfy the no-slip conditions at the wall. In order to determine the solution of the problem which accounts for the wall effects, the full Navier–Stokes equations have to be considered.

3. Similarity solution for the velocity and temperature fields over entire region

3.1. *Problem formulation*

Consider now a problem analogous to Stokes' first problem for an inclined drop impact onto a solid semi-infinite substrate accounting for the heat convection in the spreading lamella, heat conduction in the substrate and possible phase transition initiated at their contact region. The possible phase transition phenomena include wall remelting, drop solidification or vaporization. The initial temperatures of the drop, T_{d0}, and of the substrate, T_{w0}, are assumed to be uniform.

Let us determine a viscous flow $\boldsymbol{v} = u\boldsymbol{e}_x + v\boldsymbol{e}_y + w\boldsymbol{e}_z$ and the temperature distribution T in the spreading lamella and in the wall which satisfy the following initial and boundary conditions:

$$(\boldsymbol{v} - \boldsymbol{v}_0) \times \boldsymbol{e}_z = 0, \quad T = T_{d0} \quad \text{at } z \to \infty \ \forall\, t > 0 \quad \text{and at } t = 0 \ \forall z > 0, \tag{3.1a}$$

$$\boldsymbol{v} = 0, \quad T = T_{w0} \quad \text{at } z \to -\infty \ \forall\, t > 0 \quad \text{and at } t = 0 \ \forall z < 0, \tag{3.1b}$$

where $\boldsymbol{v}_0$ is the remote asymptotic solution determined in (2.3). It should be noted that only the tangential, x and y components of the velocities $\boldsymbol{v}$ and $\boldsymbol{v}_0$ must be identical far from the wall surface at $z \to \infty$, since the viscous boundary layer developed near the wall–liquid interface and the propagation of the phase transition front can generate an additional uniform flow in the vertical z direction.

The near-wall matching and jump conditions for the temperature field and for the velocity are determined by the phenomena occurring during the liquid–wall contact. They can be different depending on whether drop spreading is followed by phase transition or not. Consider a solid–fluid or fluid–fluid interface $z = Z^*(t)$. The matching conditions represent the mass, momentum and energy balance at the interface, the continuity of the shear stresses and temperature and the no-slip condition. The matching conditions are slightly different depending on whether there is no phase transition at the interface $z = Z^*$,

$$\boldsymbol{v} = 0, \quad \Delta\boldsymbol{\phi}_q = 0, \quad \Delta(\boldsymbol{\sigma} \cdot \boldsymbol{e}_z) = 0, \quad \Delta T = 0, \tag{3.2}$$

or the moving interface $z = Z^*(t)$ corresponds to a phase change,

$$\rho(\boldsymbol{v} \cdot \boldsymbol{e}_z - \dot{Z}^*) = -\frac{\Delta\boldsymbol{\phi}_q}{\pm L} = \dot{m}, \quad \Delta(\boldsymbol{\sigma} \cdot \boldsymbol{e}_z) = \dot{m}\Delta(\boldsymbol{v} \cdot \boldsymbol{e}_z - \dot{Z}^*)\boldsymbol{e}_z, \tag{3.3a}$$

$$T = T^*, \quad \Delta(\boldsymbol{v} \times \boldsymbol{e}_z) = 0, \tag{3.3b}$$

where $\boldsymbol{\sigma}$ is the stress tensor, $\boldsymbol{\phi}_q$ is the heat flux. A jump of a physical quantity $\boldsymbol{x}$ through the interface $z = Z^*(t)$ is defined here by $\Delta\boldsymbol{x} = \boldsymbol{x}(Z^+) - \boldsymbol{x}(Z^-)$.

In the absence of the phase transition at the interface $z = Z^*$ the temperature T^* has to be determined from the solution, while the instantaneous phase transition rate is equal to zero, $\dot{m} = 0$.

If $z = Z^*(t)$ represents a moving phase transition front, the temperature T^* is a thermodynamic property equal to the melting or boiling temperature (depending on whether solidification, melting or evaporation takes place at the interface). The local mass rate of phase transition $\dot{m}$ in this case is not known *a priori* and has to be determined from the solution. The value of L is equal to the latent heat of fusion or latent heat of evaporation per unit mass, depending on the kind of phase transition at the interface $z = Z^*(t)$. The sign near L in the first expression (3.3*a*) is positive in the case of liquid solidification or negative in the case of the substrate remelting or liquid evaporation.

The flow and the temperature fields in the spreading drop have to satisfy the continuity, momentum and energy balance equations (Bird, Stewart & Lightfoot 1960)

$$\frac{\partial \rho}{\partial t} + \nabla \cdot (\rho \boldsymbol{v}) = 0, \tag{3.4a}$$

$$\rho \frac{\partial \boldsymbol{v}}{\partial t} + \rho\,(\boldsymbol{v} \cdot \nabla)\,\boldsymbol{v} = -\nabla p + \nabla \cdot \left(\mu \left[\nabla \boldsymbol{v} + \nabla \boldsymbol{v}^T \right] - \frac{2}{3}\mu (\nabla \cdot \boldsymbol{v}) \boldsymbol{I} \right), \tag{3.4b}$$

$$\rho c_v \left(\frac{\partial T}{\partial t} + \boldsymbol{v} \cdot \nabla T \right) = \nabla \cdot (k \nabla T), \tag{3.4c}$$

where $\boldsymbol{I}$ is the unity tensor.

The viscosity, density, specific heat and thermal conductivity: $\mu = \mu(T)$, $\rho = \rho(T)$, $c_v = c_v(T)$, $k = k(T)$, depend on the local temperature, on the local phase and material.

3.2. *Similarity solution*

We seek a solution in the following form, determined by the remote asymptotic solution (2.3):

$$\boldsymbol{v} = f(\xi)\,\frac{(x + U_0\tau)\boldsymbol{e}_x + y\boldsymbol{e}_y}{t} - 2g(\xi)\frac{\sqrt{\nu_0}}{\sqrt{t}}\,\boldsymbol{e}_z, \tag{3.5a}$$

$$T = T_{w0} + (T_{d0} - T_{w0})\,\Theta(\xi), \tag{3.5b}$$

where the dimensionless similarity variable is defined as

$$\xi = \frac{z}{\sqrt{\nu_0 t}}. \tag{3.6}$$

Here ν_0 is the constant characteristic viscosity of liquid and $\sqrt{\nu_0 t}$ is the typical viscous length.

For convenience we also define a local dimensionless temperature coefficient of a physical property x as

$$\mathscr{A}_x(T) = (T_{d0} - T_{w0})\frac{1}{x}\frac{\mathrm{d}x}{\mathrm{d}T}. \tag{3.7}$$

Since we consider variable material properties which depend on the temperature but also on the local phase state and material, our similarity solution has to be applicable to the entire field, which includes spreading liquid lamella, solid wall and the intermediate region appearing as a result of the phase transition. The velocity field

and the temperature distribution have to satisfy the following boundary conditions:

$$f = 1, \quad \Theta = 1, \quad \frac{\partial p}{\partial x} = \frac{\partial p}{\partial y} = 0, \quad \text{at } \xi \to \infty, \tag{3.8a}$$

$$f = g = 0, \quad \Theta = 0, \quad \text{at } \xi \to -\infty. \tag{3.8b}$$

The z component of the Navier–Stokes equations (3.4b) together with the boundary conditions (3.8) immediately yield the form for the pressure field in the lamella:

$$p = \nu_0 \rho P(\xi)/t + P_1(t), \tag{3.9}$$

where the scaled pressure $P(\xi)$ can be evaluated integrating the ordinary differential equation

$$P' + P\mathscr{A}_\rho \Theta' + g + \xi g' + 4gg' + \frac{2\nu}{3\nu_0}\left[2\mathscr{A}_\mu \Theta'(f + 2g') + 4g'' - f'\right] = 0, \tag{3.10}$$

$\nu(T)$ being the local kinematic viscosity.

Since the pressure gradients in the x and y directions vanish, the corresponding components of the Navier–Stokes equations (3.4b) can be simplified. The continuity equation (3.4a), the energy equation (3.4c) and the Navier–Stokes equations (3.4b) in the x and y directions can be rewritten in terms of the similarity variable ξ:

$$f - g' - \frac{\mathscr{A}_\rho}{4}(\xi + 4g)\Theta' = 0, \tag{3.11}$$

$$\Theta'' + \mathscr{A}_k \Theta'^2 + \frac{Pr}{2}(\xi + 4g)\Theta' = 0, \tag{3.12}$$

$$-f + f^2 - \frac{f'}{2}(\xi + 4g) - \frac{\nu}{\nu_0}(\mathscr{A}_\mu f'\Theta' + f'') = 0, \tag{3.13}$$

where the prime denotes the differentiation with respect to ξ and $Pr(T) = \nu_0 \rho c_v / k$ is the local Prandtl number. It should be noted that the scaled x and y components of the Navier–Stokes equation lead to the same expression (3.13). This is a lucky coincidence which allows us to describe axisymmetric and three-dimensional time-dependent flows (3.5) generated by normal or oblique drop impacts using the same similarity solution.

Equations (3.11)–(3.13) form a system of ordinary differential equations for the scaled velocities, $g(\xi)$ and $f(\xi)$, and temperature, Θ, which can be easily solved numerically if the material properties and their temperature dependencies are known and if the boundary conditions near the wall surface are defined. Several examples of various physical processes which can follow the lamella spreading are shown in figure 2. The interface of phase transition is defined by $\xi = \Xi^*$, where Ξ^* is a constant which has to be determined from the solution.

The matching conditions are obtained from (3.2) for a solid–fluid or solid–solid interface $\xi = 0$ without phase transition,

$$g = 0, \quad f = 0, \quad \Delta(k\Theta') = 0, \quad \Delta\Theta = 0, \tag{3.14}$$

and the corresponding conditions for a fluid/fluid interface are

$$g = 0, \quad \Delta f = 0, \quad \Delta(\mu f') = 0, \quad \Delta(k\Theta') = 0, \quad \Delta\Theta = 0. \tag{3.15}$$

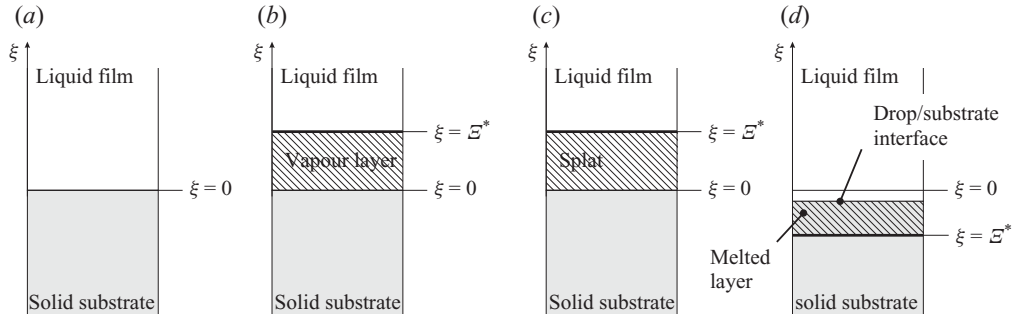

FIGURE 2. Examples of various thermodynamic processes following film spreading and interfaces between different regions: (*a*) spreading without phase transition, (*b*) film boiling, (*c*) film solidification and (*d*) target melting. Interfaces with phase transition determined by $\xi = \Xi^*$ are shown by bold lines.

The matching and jump conditions for a moving solid–fluid boundary $\xi = \Xi^*$ with phase change are obtained from (3.3) in the following form:

$$\rho\left(2g + \frac{\Xi^*}{2}\right) = -\frac{T_{d0} - T_{w0}}{\pm L\nu_0}\Delta(k\Theta'), \tag{3.16a}$$

$$\Theta = \frac{T^*}{T_{d0} - T_{w0}}, \quad f = 0. \tag{3.16b}$$

The corresponding matching and jump conditions at a moving fluid–fluid boundary $\xi = \Xi^*$ with phase change are

$$\rho\left(2g + \frac{\Xi^*}{2}\right) = -\frac{T_{d0} - T_{w0}}{\pm L\nu_0}\Delta(k\Theta'), \quad \Delta(\mu f') = 0, \tag{3.17a}$$

$$\Theta = \frac{T^*}{T_{d0} - T_{w0}}, \quad \Delta f = 0. \tag{3.17b}$$

In all the considered cases the similarity conditions are satisfied, since the variables x, y, z and t do not explicitly appear in our expressions.

It should be noted that generally non-zero velocity field exists in the solid regions, resulting from the thermal expansion. The velocity field in the solid is determined by the temperature field and the thermal expansion coefficient, as well as by the elastic and plastic properties of the material. These velocities, however, are usually much smaller than the typical drop velocity and can be neglected in the present analysis.

4. Drop impact with solidification, constant thermophysical properties of materials

Consider a simple particular case of drop impact with solidification, in which the dependence of the material properties of drop, solder and target on temperature is negligible. In the case when the thermophysical properties are independent of T, the system (3.11)–(3.13) reduces to the following form valid for all three regions:

$$f = g', \tag{4.1a}$$

$$\Theta'' + \frac{Pr}{2}(\xi + 4g)\Theta' = 0, \tag{4.1b}$$

$$g''' + 2gg'' + \frac{1}{2}\xi g'' + g' - g'^2 = 0. \tag{4.1c}$$

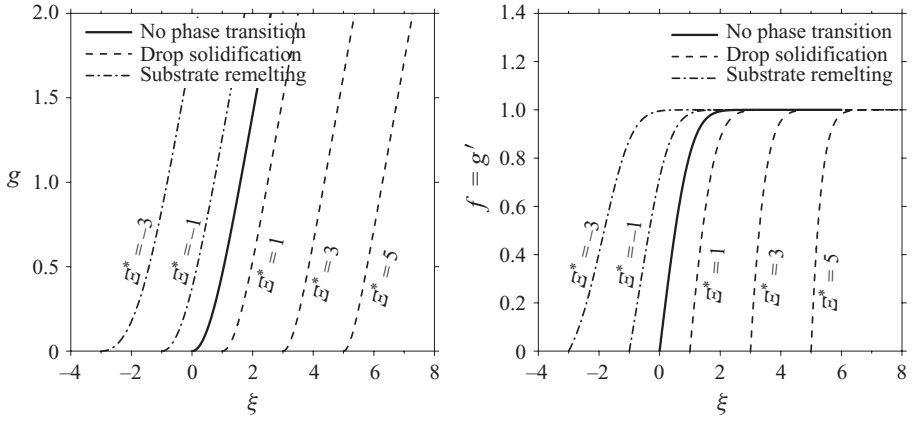

FIGURE 3. Scaled components of the velocity of the liquid with phase transition at various position of the interface $\xi = \Xi^*$ obtained by the numerical integration of (4.1c).

Equation (4.1c) for the scaled velocity is identical to the corresponding self-similar solution obtained in Roisman (2009).

We can subdivide the entire domain into three regions: solid target $g = g' = 0$ at $\xi \in]-\infty, 0]$, solder ($g = g' = 0$) at $\xi \in [0, \Xi^*]$ and spreading liquid film at $\xi \in [\Xi^*, \infty[$ (see figure 2c).

For simplicity we also neglect the change of the density of the drop material during solidification.

4.1. *The flow and the temperature distribution in the liquid drop*

For the liquid flow, $\xi > \Xi^*$, (4.1c) can be easily solved numerically subject to the boundary conditions:

$$g = g' = 0 \quad \text{at } \xi = \Xi^* \quad \text{and} \quad g' = 1 \quad \text{at } \xi \to \infty. \tag{4.2}$$

In figure 3 the results of the numerical calculations of the scaled velocities g and g' are shown for various values of Ξ^*. Each curve intersects the axis $g = 0$ (or respectively $g' = 0$) at $\xi = \Xi^*$.

It can be shown that the scaled velocity g behaves like

$$g \to \xi - \Xi^* - \gamma(\Xi^*) \quad \text{at } \xi \to \infty, \tag{4.3}$$

where the constant γ depends only on the position of the interface $\xi = \Xi^*$ and has to be found from the numerical solution of (4.1c). The value of $\Xi^* + \gamma(\Xi^*)$ corresponds to a uniform vertical flow generated by an expansion of the viscous boundary layer and propagation of the solidification front. In figure 4 the numerical predictions of γ are shown as a function of Ξ^*.

For convenience this function can be fitted by an exponential function of Ξ^* and written in an explicit form:

$$\gamma \approx \frac{0.290}{\exp[0.351\,\Xi^*]} + \frac{0.314}{\exp[0.0599\,\Xi^*]}. \tag{4.4}$$

Approximation (4.4) is valid on the interval $\Xi^* \in [-3, 15]$ and is used in subsequent calculations of the temperature field.

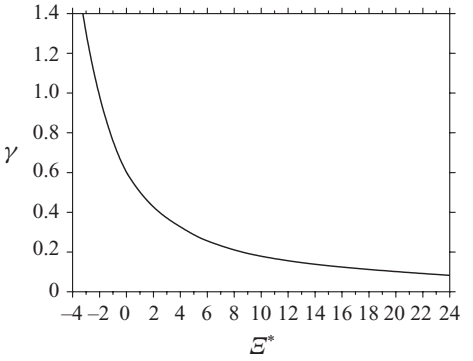

FIGURE 4. Calculated values of γ defined in (4.3) at various values of Ξ^*.

A general solution for the temperature field in the liquid drop is determined from (4.1*b*):

$$\Theta = C_1 + C_2 \mathscr{I}(Pr, \Xi^*, \xi), \tag{4.5a}$$

$$\mathscr{I}(Pr, \Xi^*, \xi) = \frac{\sqrt{Pr}}{\sqrt{\pi}} \int_{\Xi^*}^{\xi} \exp\left[-\frac{Pr}{4}\chi^2 - 2Pr \int_{\Xi^*}^{\chi} g(\zeta)\mathrm{d}\zeta\right] \mathrm{d}\chi, \tag{4.5b}$$

where C_1 and C_2 are integration constants, $Pr = \nu\rho c_v/k$ is the Prandtl number, and ζ and χ are dummy variables.

The temperature at the interface $\xi = \Xi^*$ is equal to the melting point temperature. Therefore the scaled temperature distribution in the liquid drop which satisfies the boundary conditions (3.8*a*) is

$$\Theta_l(\xi) = \Theta^* + (1 - \Theta^*)\frac{\mathscr{I}(Pr_l, \Xi^*, \xi)}{\mathscr{I}(Pr_l, \Xi^*, \infty)}. \tag{4.6}$$

4.2. *Temperature distributions in the solid regions: target and splat*

A general solution for the energy equation in the solid regions can be obtained by substituting $g = 0$ in (4.5):

$$\Theta = C_3 + C_4 \mathrm{erfc}\left[\frac{-\sqrt{Pr}\xi}{2}\right], \tag{4.7}$$

where the corresponding Prandtl number is defined on the base of the viscosity of the liquid.

Let Θ_c denote the contact temperature at $\xi = 0$. The temperature distributions in the wall, Θ_w, and in the splat, Θ_s, which satisfy the boundary conditions (3.14) are

$$\Theta_w = \Theta_c \,\mathrm{erfc}\left[-\frac{\sqrt{Pr_w}}{2}\xi\right], \tag{4.8a}$$

$$\Theta_s = \Theta_c + (\Theta^* - \Theta_c)\frac{\mathrm{erf}\left[\dfrac{\sqrt{Pr_s}}{2}\xi\right]}{\mathrm{erf}\left[\dfrac{\sqrt{Pr_s}}{2}\Xi^*\right]}, \tag{4.8b}$$

where

$$\Theta_c = \frac{e_s \Theta_z}{e_s + e_w \,\mathrm{erf}\left[\dfrac{\sqrt{Pr_s}\,\Xi^*}{2}\right]}. \tag{4.8c}$$

Here, $e_s = \sqrt{k_s \rho_s c_s}$ and $e_w = \sqrt{k_w \rho_w c_w}$ are the thermal effusivities of the splat and wall, respectively.

At this stage only the value of Ξ^* is not known. It has to be determined from the boundary conditions related to phase change, in particular from the local heat balance at the solidification front.

4.3. *Drop solidification*

The boundary conditions (3.16) for the temperatures Θ_l and Θ_s in the liquid and splat regions yield

$$\Xi^* = \frac{2Ste}{Pr_l}\left[\frac{k_s}{k_l}\Theta_s'(\Xi^*) - \Theta_l'(\Xi^*)\right], \tag{4.9a}$$

$$Ste = \frac{c_{pl}(T_{d0} - T_{w0})}{L}, \tag{4.9b}$$

where Ste is the Stefan number and L is the latent heat of fusion per unit mass.

Finally, expression (4.9) with the help of (4.6) and (4.8) yields the following transcendental integral equation for Ξ^*:

$$\frac{k_s}{k_l}\mathscr{S}\Theta^* - \mathscr{L}(1 - \Theta^*) = \frac{Pr_l\sqrt{\pi}}{2Ste}\Xi^*, \tag{4.10a}$$

where

$$\mathscr{L} = \frac{\sqrt{Pr_l}\exp\left[-\dfrac{Pr_l}{4}\Xi^{*2}\right]}{\mathscr{I}(Pr_l, \Xi^*, \infty)}, \tag{4.10b}$$

$$\mathscr{S} = \frac{e_w\sqrt{Pr_s}\exp\left[-\dfrac{Pr_s}{4}\Xi^{*2}\right]}{e_w \mathrm{erf}\left[\dfrac{\sqrt{Pr_s}}{2}\Xi^*\right] + e_s}. \tag{4.10c}$$

This equation can be solved numerically if all the thermophysical parameters are known.

Function $\mathscr{L}(Pr_l, \Xi^*)$ in (4.10) is not given in an explicit form since it involves the integral function $\mathscr{I}(Pr_l, \Xi^*, \infty)$, which depends on the scaled velocity $g(\xi)$. On the other hand, it can be easily evaluated for given Pr and Ξ^*. The results of calculations of $\mathscr{L}(Pr_l, \Xi^*)$ are shown in figure 5 for various Prandtl numbers. For each Prandtl number the function $\mathscr{L}(Pr_l, \Xi^*)$ is a monotonously increasing function of Ξ^*. Negative values of Ξ^* correspond to the case of remelting of the substrate if it is of the same material as the impacting liquid drop.

The dimensional height Z^* of the solidification front increases in time and can be expressed as

$$Z^* = \Xi^*\sqrt{\nu t}. \tag{4.11}$$

4.4. *Drop impact without phase transition*

Using the boundary conditions (3.8) and (3.14) in (4.5) and noting that $g = 0$ at $\xi < 0$, the following expressions for the temperature fields Θ_l and Θ_w in the liquid and solid

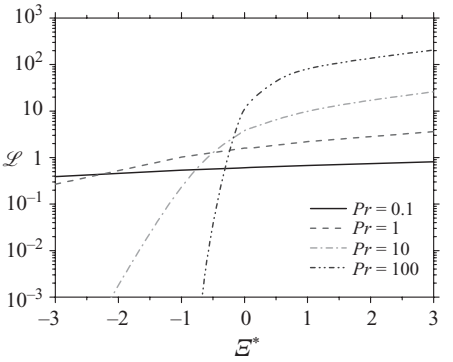

FIGURE 5. Function $\mathscr{L}(Pr, \Xi^*)$, defined in (4.10*b*), as a function of Ξ^* for various Prandtl numbers.

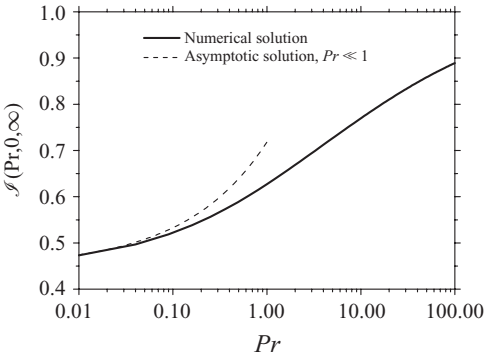

FIGURE 6. Function $\mathscr{I}(Pr, \infty)$ for the liquid phase as a function of the Prandtl number, calculated using (4.5*b*), in comparison with the approximate solution (4.16) for small Prandtl numbers.

regions are obtained:

$$\Theta_l = \frac{e_l + e_s \mathscr{I}(Pr_l, 0, \xi)}{e_l + e_s \mathscr{I}(Pr_l, 0, \infty)} \quad \text{at } \xi > 0, \tag{4.12a}$$

$$\Theta_w = \frac{e_l}{e_l + e_w \mathscr{I}(Pr_l, 0, \infty)} \operatorname{erfc}\left[-\frac{\sqrt{Pr_w}}{2}\xi\right] \quad \text{at } \xi < 0. \tag{4.12b}$$

The corresponding dimensional contact temperature at $z = 0$ can now be determined by

$$T_c = \frac{e_l T_{d0} + e_w \mathscr{I}(Pr_l, 0, \infty) T_{w0}}{e_l + e_w \mathscr{I}(Pr_l, 0, \infty)}, \tag{4.13}$$

and the heat flux at the interface $z = 0$ is

$$\phi_q = \frac{e_l e_w (T_{w0} - T_{d0})}{[e_l + e_w \mathscr{I}(Pr_l, 0, \infty)]\sqrt{\pi}\sqrt{t}}. \tag{4.14}$$

Dimensionless function $\mathscr{I}(Pr, 0, \infty)$ defined in (4.5*b*) can be calculated numerically for various Prandtl numbers. The results of calculations are shown in figure 6. On the entire range of the Prandtl numbers the value of $\mathscr{I}(Pr, 0, \infty)$ is smaller than unity. In the limiting case $Pr \to \infty$ (instantaneous contact of two solid semi-infinite bodies),

Material	Density	Thermal conductivity	Specific heat	Latent heat of fusion	Dynamic viscosity	Melting point
	ρ (kg m^{-3})	k (W m^{-1} K^{-1})	(c) (J kg^{-1} K^{-1})	h (J kg^{-1})	μ (N s m^{-2})	°C
Tin (liquid)	6970	33.6	243	60.9×10^3	1.917×10^{-3}	–
Tin (solid)	6970	59.6	243	60.9×10^3	–	232.06
Stainless steel	8055	15.1	480	–	–	1370–1400

TABLE 1. Thermophysical properties of materials used.

the value of $\mathscr{I}(Pr,\infty)$ approaches unity. These results explain the enhanced cooling effect of drop or spray impact.

For very small Prandtl numbers, typical for liquid metals, the flow viscosity can be neglected, the scaled velocity $g(\xi)$ can thus be approximated by its outer asymptotic solution $\xi-\Xi^*-\gamma(\Xi^*)$, determined in (4.3), and the function $\mathscr{I}(Pr_l,\Xi^*,\infty)$ can be estimated using (4.5b) by

$$\mathscr{I}(Pr_l,\Xi^*,\infty)=\frac{\sqrt{Pr_l}}{\sqrt{\pi}}\int_{\Xi^*}^{\infty}\exp\left[-\frac{Pr_l}{4}\chi^2-2Pr_l\int_{\Xi^*+\gamma}^{\chi}(\zeta-\Xi^*-\gamma)\mathrm{d}\zeta\right]\mathrm{d}\chi$$
$$=\frac{\sqrt{5}}{5}\exp\left[-\frac{Pr_l}{5}(\Xi^*+\gamma)^2\right]\mathrm{erfc}\left[\frac{\sqrt{Pr_l}}{2\sqrt{5}}(\Xi^*-4\gamma)\right] \tag{4.15}$$

Linearization of (4.15) with respect to small Prandtl numbers yields

$$\mathscr{I}(Pr,0,\infty)\approx\frac{1}{\sqrt{5}}+\frac{4\gamma(0)\sqrt{Pr_l}}{5\sqrt{\pi}},\quad \gamma(0)\approx0.6. \tag{4.16}$$

As shown in figure 6, the approximate solution (4.16) agrees well with the numerical solution for the Prandtl numbers $Pr_l<0.1$.

5. Results and discussions

Consider an impact of a molten tin drop onto a thick stainless steel target. The corresponding experimental results can be found in Aziz & Chandra (2000) and will be used in this study for the theory validation. The thermophysical properties of these materials are listed in table 1. Most of these data are taken from Dhiman & Chandra (2005). The data for the thermal conductivity of solid tin are taken from open sources (eFunda, Engineering fundamentals, www.eFunda.com).

In experiments of Aziz & Chandra (2000), a tin liquid drop impacts onto a stainless steel substrate. The drop temperature at the instant of impact is $T_{d0}=236$°C. The initial temperature of the substrate T_{w0} has been varied in the experiments in the range $T_{w0}\in[25°\mathrm{C},200°\mathrm{C}]$. The measured contact temperature at the substrate surface is much smaller than the theoretical predictions based on the temperature distribution by heat conduction in two semi-infinite solid bodies instantaneously put in contact. The process is assumed to be inert. Since the typical times of drop impact are rather small, any additional processes, such as solute diffusion or intermetallic compound formation, are not relevant to the considered problem.

In figure 7 the theoretically predicted jump of the contact temperature T_c-T_{w0} at $\xi=0$ is compared with the experimental data from Aziz & Chandra (2000) for various drop impact velocities W_0. Since the Prandtl number of the liquid drop, $Pr_l=0.0139$, is much smaller than unity, the approximate expression (4.15) has been

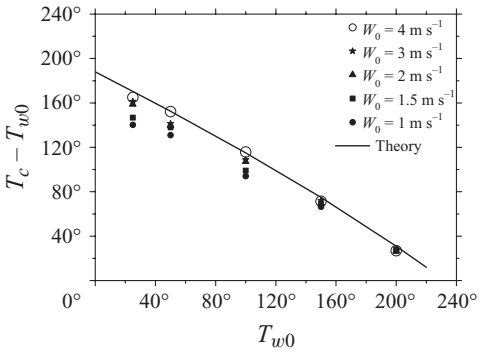

FIGURE 7. Spreading of a tin solidifying drop on a stainless steel substrate. Maximum increase of the surface temperature for various initial substrate temperatures T_{w0}. Comparison of the experimental data (Aziz & Chandra 2000) with the theoretical predictions. The drop initial temperature is $T_{d0} = 236°\mathrm{C}$.

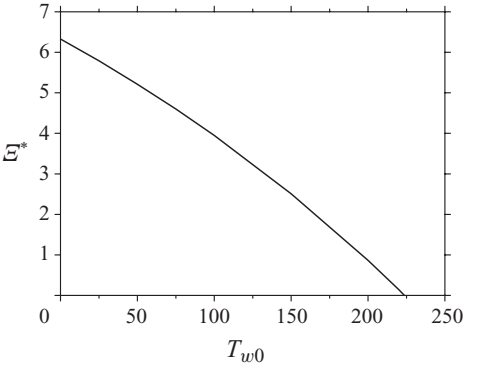

FIGURE 8. Spreading of a tin solidifying drop on a stainless steel substrate. Dependence of the scaled position of the solidification front Ξ^* on the initial substrate temperature T_{w0}. The drop initial temperature is $T_{d0} = 236°\mathrm{C}$.

used for the estimation of the function $\mathcal{I}(Pr, 0, \infty)$. The agreement between the theoretical predictions and the experimental data are rather good for the relatively high-impact velocities $W_0 \geqslant 2\,\mathrm{m\,s^{-1}}$, corresponding to the high values of the Weber number ($We \sim 10^2$) relevant to the present study. Some decrease of the measured contact temperature at smaller impact velocities can be explained by the increased influence of capillary effects at impact with smaller Weber numbers ($We \sim 10$).

In figure 8 the theoretical predictions for the scaled solidification front are shown as a function of the initial substrate temperature. The value of Ξ^* reduces as the initial temperature of the substrate increases. This is a consistent result since the lower initial temperature of the substrate enhances the rate of drop solidification.

Now consider the impact of a liquid drop onto a solid substrate of the same material. This case is relevant to spray coating or ice accretion on plane wings by the impact of supercooled drops. In figure 9 the theoretically predicted values of Ξ^* are shown as a function of the drop temperature for various initial temperatures of the substrate for the impact of a liquid tin drop onto a solid tin substrate. The substrate remelting (Ξ^*) occurs at higher drop temperatures.

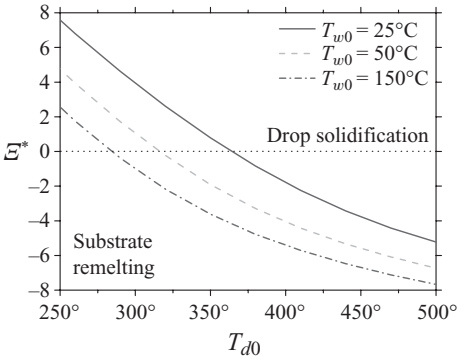

FIGURE 9. Spreading of a liquid tin drop on a solid tin substrate. Estimated values of the scaled front of phase transition at various drop and substrate temperatures. $\Xi^* > 0$ corresponds to the drop solidification and $\Xi^* < 0$ corresponds to the substrate remelting.

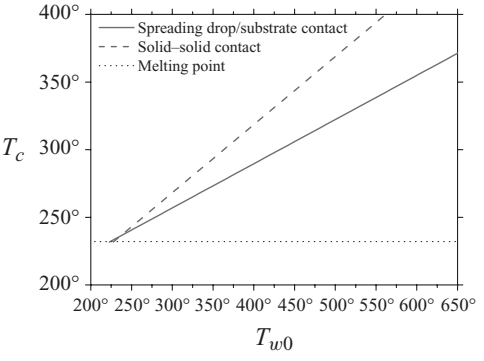

FIGURE 10. Spreading of a tin drop on a stainless steel substrate without phase transition. Theoretically predicted contact temperature T_c in comparison with the solid–solid contact temperature calculated using $\mathcal{I}(Pr, 0, \infty) = 1$. The drop initial temperature is $T_{d0} = 236°C$.

If the contact temperature predicted by (4.13) is higher than the melting point the drop will not start to solidify. This case is shown in figure 10 for spreading of a liquid tin drop on a solid stainless substrate. In this figure the theoretically predicted contact temperature is compared with the solid–solid contact temperature, calculated using $\mathcal{I}(Pr, 0, \infty) = 1$, which is frequently used in the analysis of thermal effects associated with drop impact. The difference between these two temperatures is significant, which indicates the enhanced cooling effect of the liquid flow in the spreading drop.

At relatively long times after impact, the viscous and the thermal boundary layers reach the upper free surface of the deforming drop. At this instant the boundary conditions at this drop interface are not satisfied by our solution, which is therefore no longer valid. Viscous forces lead to the quick velocity deceleration and formation of a residual liquid film (Bakshi *et al.* 2007; Roisman 2009), even in the absence of solidification. Nevertheless, the processes occurring during the earlier stages of drop spreading, described in this study, often determine the residual film thickness and its maximum diameter, geometry of splat and drop impact outcome.

It should be noted that the theory developed in this paper is based on a purely analytical solution of the spreading problem relevant to drop impact with the relatively high Reynolds and Weber numbers. In the present stage it does not account for some

more complicated physical phenomena associated with phase transition, such as homogeneous nucleation, kinetic effects in phase transition, diffusion or oxidation of the materials, radiative heat transfer, flow instability leading to drop breakup or formation of a rough, porous splat, etc. However, it is obvious that this solution can be potentially used as a base flow for investigation of these important phenomena.

6. Conclusions

This study is devoted to the analysis of a fast forced non-axisymmetric spreading of a liquid film generated by inclined drop impact onto a solid flat substrate. A similarity solution for the combined full Navier–Stokes equations and energy equations is obtained which allows us to predict the viscous flow and the temperature distribution in the film even if the thermophysical parameters of the liquid and solid materials depend on the temperature. The theory also allows us to describe the phase transition initiated by drop impact and spreading, including drop solidification near the wall, substrate remelting and drop evaporation. In the case of temperature-independent thermophysical properties this theory predicts the rate of propagation of the phase change front as a function of time, liquid viscosity, the Stefan and Prandtl numbers.

The theoretical predictions of the contact temperature in the case of drop solidification agree well with the available experimental data. We have shown that this temperature significantly differs from the well-known value of the contact temperature based on the analysis of heat conduction in two solid bodies instantaneously put in contact.

The theory has a wide range of industrial applications. These applications include the modelling of thermal spray coating and forming, ice accretion and inkjet printing.

The author acknowledges financial support from the EU FP7 ‘EXTICE’ Project.

REFERENCES

Amon, C. H., Schmaltz, K. S., Merz, R. & Prinz, F. B. 1996 Numerical and experimental investigation of interface bonding via substrate remelting of an impinging molten metal droplet. *J. Heat Trans.* **118**, 164–172.

Attinger, D., Zhao, Z. & Poulikakos, D. 2000 An experimental study of molten microdroplet surface deposition and solidification: transient behaviour and wetting angle dynamics. *J. Heat Trans.* **122**, 544–556.

Aziz, S. D. & Chandra, S. 2000 Impact, recoil and splashing of molten metal droplets. *Intl J. Heat Mass Trans.* **43**, 2841–2857.

Bakshi, S., Roisman, I. V. & Tropea, C. 2007 Investigations on the impact of a drop onto a small spherical target. *Phys. Fluids* **19**, 032102.

Bico, J., Marzolin, C. & Quéré, D. 1999 Pearl drops. *Europhys. Lett.* **47**, 220.

Bird, R. B., Stewart, W. E. & Lightfoot, E. N. 1960 *Transport Phenomena*. Wiley.

Carey, V. P. 2007 *Liquid Vapour Phase Change Phenomena: An Introduction to the Thermophysics of Vaporization and Condensation Processes in Heat Transfer Equipment*. Pergamon.

Dhiman, R. & Chandra, S. 2005 Freezing-induced splashing during impact of molten metal droplets with high Weber numbers. *Intl J. Heat Mass Trans.* **48**, 56255638.

Dijksman, J. F. & Pierik, A. 2008 Fluid dynamical analysis of the distribution of ink jet printed biomolecules in microarray substrates for genotyping applications. *Biomicrofluidics* **2**, 044101.

Fauchais, P., Fukumoto, M., Vardelle, A. & Vardelle, M. 2004 Knowledge concerning splat formation: an invited review. *J. Therm. Spray Technol.* **13** (3), 337–360.

Kellay, H. 2005 Impact of drops on a water-covered sand bed: erosion, entrainement and pattern formation. *Europhys. Lett.* **71** (3), 400–406.

Manzello, S. L. & Yang, J. C. 2002 On the collision dynamics of a water droplet containing an additive on a heated solid surface. *Proc. R. Soc. Lond.* A **458**, 2417–2444.

Miller, D. R., Lynch, J. & Tate, P. A. 2002 Overview of high speed close-up imaging in an icing environment. *Tech. Mem.* TM 2004-212925. NASA, *Paper 2004-0407*, Forty-second Aerospace Sciences Meeting and Exhibit, AIAA.

Mock, U., Michel, T., Tropea, C., Roisman, I. V. & Rühe, J. 2005 Drop impact on chemically structured arrays. *J. Phys.: Condens. Matter* **17**, S607–S622.

Orme, M. 1993 A novel technique of rapid solidification net-form materials synthesis. *J. Mater. Engng Perform.* **2** (3), 399–405.

Pepper, R. E., Courbin, L. & Stone, H. A. 2008 Splashing on elastic membranes: the importance of early-time dynamics. *Phys. Fluids* **20**, 082103.

Range, K. & Feuillebois, F. 1998 Influence of surface roughness on liquid drop impact. *J. Colloid Interface Sci.* **203**, 16–30.

Rein, M. (Ed.) 2000 *Drop-Surface Interactions*. Springer.

Roisman, I. V. 2009 Inertia dominated drop collisions. Part II. An analytical solution of the Navier–Stokes equations for a spreading viscous film. *Phys. Fluids* **21**, 052104.

Roisman, I. V., Berberović, E. & Tropea, C. 2009 Inertia dominated drop collisions. Part I. On the universal flow in the lamella. *Phys. Fluids* **21**, 052103.

Roisman, I. V. & Tropea, C. 2002 Impact of a drop onto a wetted wall: description of crown formation and propagation. *J. Fluid Mech.* **472**, 373–397.

Senda, J., Yamada, K., Fujimoto, H. & Miki, H. 1988 The heat transfer characteristics of a small droplet impinging upon a hot surface. *JSME Intl J.* II **31**, 105–111.

Steirer, K. X., Berry, J. J., Reese, M. O., van Hest, M. F. A. M., Miedaner, A., Liberatore, M. W., Collins, R. T. & Ginley, D. S. 2009 Ultrasonically sprayed and inkjet printed thin film electrodes for organic solar cells. *Thin Solid Films* **517**, 2781–2786.

Tropea, C. & Roisman, I. V. 2005 Droplet breakup and coalescense. In *Multiphase Flow Handbook* (ed. C. Crowe), Mechanical Engineering Series, vol. 27, ch. 12.3. CRC Press.

Ukiwe, C. & Kwok, D. Y. 2005 On the maximum spreading diameter of impacting droplets on well-prepared solid surfaces. *Langmuir* **21**, 666–673.

Worster, M. G. 2000 Solidification of fluids. In *Perspectives in Fluid Dynamics: A Collective Introduction to Current Research* (ed. G. K. Batchelor, H. K. Moffat & M. G. Worster), pp. 393–446. Cambridge University Press.

Yarin, A. L. 2006 Drop impact dynamics: splashing, spreading, receding, bouncing. *Annu. Rev. Fluid Mech.* **38**, 159–192.

Yarin, A. L. & Weiss, D. A. 1995 Impact of drops on solid surfaces: self-similar capillary waves, and splashing as a new type of kinematic discontinuity. *J. Fluid Mech.* **283**, 141–173.